Acta metall. mater. Vol. 40, No. 1, pp. 113–122, 1992
Printed in Great Britain

0956-7151/92 $5.00 + 0.00
Pergamon Press plc

INTERGRANULAR FRACTURE OF FAST REACTOR IRRADIATED STAINLESS STEEL

I. J. FORD

Theoretical Studies Department, Materials and Manufacturing Technology Division, AEA Industrial Technology, Harwell Laboratory, Didcot, Oxon OX11 0RA, England

(Received 7 September 1990; in revised form 24 May 1991)

Abstract—A mechanistic understanding of the failure of fuel pins in a Fast Reactor, in normal operation or in accident conditions, is very important in assessing safety. Progress in gaining such an understanding has been slow and greater emphasis has been placed on empirical failure rules. This paper presents a simple set of physical models describing the intergranular fracture of Fast Reactor irradiated stainless steel fuel pin cladding. The approach emphasizes the importance of both the nucleation and growth of intergranular cavities as well as the effects of helium bubble formation during irradiation. The models allow a unified theoretical approach to be taken in describing unirradiated, in-pile and post-irradiation creep rupture experiments, as well as Fuel Cladding Transient Tests (FCTT).

Résumé—Pour mieux estimer la sûreté des réacteurs à neutrons rapides il est très important de comprendre au niveau mécaniste la rupture des aiguilles combustibles en régime normal et au cas d'un accident. Les progrès vers cet idéal ont été peu rapides, et on a fait appel plutôt aux règles empiriques. Cet exposé présente un simple ensemble de modèles physiques décrivant la rupture intergranulaire dans un acier inoxydable de gainage irradié dans un réacteur rapide. La méthode fait ressortir le rôle de la germination et la croissance des cavités intergranulaires en plus des effets des bulles d'hélium provenant de l'irradiation. Les modèles permettent un traitement théorique uniforme des essais de fluage faits avant, pendant ou après une irradiation, et aussi des essais de gaines à puissance transitoire.

Zusammenfassung—Bei der Sicherheitsanalyse eines schnellen Reaktors hat die mechanistische Erklärung des Versagens der Brennstäbe sowohl im Normalbetrieb als auch in Störfällen eine wichtige Rolle zu spielen. In dieser Richtung aber ist nur langsam fortgeschritten und man ist vielmehr auf empirische Regeln angewiesen, In der vorliegenden Arbeit wird eine einfache Sammlung physikalischer Modelle vorgestellt, die die Entwicklung des Korngrenzenbruches in Brennstabhüllen aus Edelstahl unter Bestrahlung in einem schnellen Reaktor beschreiben. Bei dieser Betrachtungsweise stehen nicht nur die Effekte der durch Bestrahlung erzeugten Heliumblasen sondern auch die Keimbildung und das Wachstum der intergranulären Hohlräumen im Vordergrund. Die Modelle gestatten eine einheitliche theoretische Betrachtung von Zeitstandversuchen wie sie vor, während oder nach einer Reaktorbestrahlung ausgeführt werden sowie von Leistungstransiente-Versuchen an Brennstabhüllen.

1. INTRODUCTION

The material used to clad fuel pins in a nuclear reactor constitutes the primary barrier against the release of radioactive fission products from the core. In the unlikely event of an accident which leads to cladding fracture, the location and timing of the failure strongly affects the severity of the incident, due to the associated fuel motion and core reactivity feedback effects. The fracture of reactor cladding materials has therefore received a great deal of experimental and theoretical investigation. Neutron irradiation usually leads to a marked loss in ductility compared to the unirradiated material, but experiments are difficult due to the radiation protection considerations and expense of facilities [1]. This paper describes a set of simple models of the physical processes underlying mechanical fracture of cladding, which aim to interpret this hard-won data. The models are intended for use in computer codes which describe fuel pin behaviour (such as TRAFIC [2] and TRANSURANUS [3]) and codes which simulate whole core accidents (for instance EAC2 [4]). We have concentrated on fracture mechanisms in Fast Reactor irradiated fuel pins, but the mechanistic basis of the models should allow extension to thermal reactors.

Hitherto, pin failure modelling has relied largely on the use of empirical rules to describe mechanical fracture [5, 6]. The plethora of fracture rules, their mutual inconsistencies and limited ranges of validation, together with the lack of identification of individual fracture mechanisms, have been seen as weaknesses. Thus there is strong motivation for developing mechanistic models. The models should be founded on a few physical mechanisms each dealing with specific fracture models. Failure in operational conditions should be understood as well as in accident conditions and the models must be based on sets of differential equations so that the time dependence is fully accounted for.

Identifying the important modes of fracture provides a considerable simplification [7]. Figure 1 is a

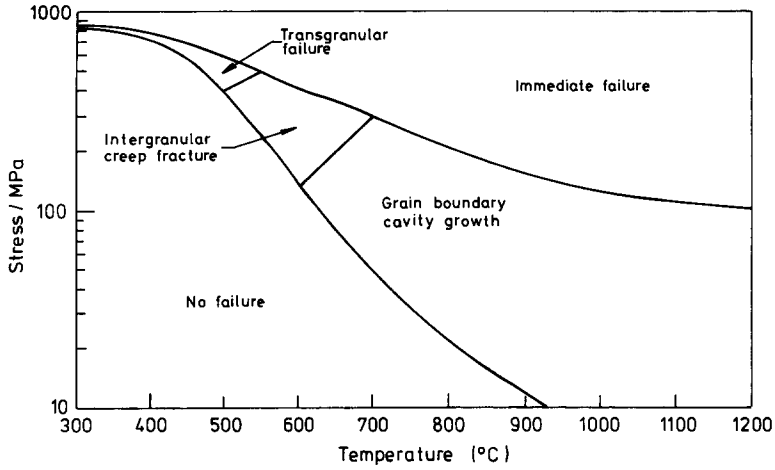

Fig. 1. Schematic failure mechanism map for 316 steel.

fracture map for the cladding material we concentrate on here, 20% cold worked AISI 316 steel, illustrating ranges of cladding temperature and stress conditions in which particular mechanisms are responsible for failure. The diagram is schematic: history dependence is ignored, failure times are not indicated and the boundaries between regions are uncertain. However, it serves to introduce the three main fracture mechanisms we shall consider:

1.1. Transgranular failure

This mechanism breaks into two sub-types, channel fracture and growth of intragranular cavities [8]. Both are ductile failure processes and are commonly seen in irradiated stainless steels tested at the lower end of the temperature range. In both mechanisms the failure is produced by local plastic flow and is characterised by a yield stress and a fixed stress limit, or ultimate tensile stress.

1.2. Intergranular creep fracture

In this mechanism grain boundary cracks are nucleated and grow during deformation. Helium gas, generated by (n, α) reactions with certain constituents of the cladding, is thought to play a role but grain boundary cavities are not necessarily present. Once nucleated the cracks grow by interlinkage until a critical crack length is reached. No fixed stress limit is associated with this mechanism but failure is strongly correlated with creep strain.

1.3. Grain boundary cavity growth

For higher temperatures and lower stresses, grain boundary cavity growth becomes important. After irradiation, He gas provides bubbles as nuclei for the cavities. the bubbles have to be greater than a critical size for a given load to grow. No fixed stress limit applies.

The main distinction between these failure modes is the relationship between the fracture surface and the grain structure. Our modelling of the transgranular fracture mode is dealt with elsewhere [8, 9]: here we concentrate on the intergranular modes (ii) and (iii). We therefore confine ourselves to high temperature rupture data where thermal creep is the main source of cladding deformation. We take a unified view that the two intergranular failure modes can be described in terms of the same underlying physics: the nucleation and growth of grain boundary decohesions driven by grain boundary sliding due to creep. The formation of cracks rather than cavities is determined by the pattern of nucleation on the grain boundaries. We will expand on these details later, but first, in Section 2, we examine the mechanisms of growth of cavities once they have been formed. In Section 3 the question of nucleation is dealt with, including the effects of helium bubbles on the grain boundaries, which are themselves considered at greater length in Section 4. Some example calculations with the models are given in Section 5, and our conclusions appear in Section 6. The appendix provides a nomenclature.

2. CAVITY GROWTH

Cavity growth laws have been the subject of study for over 30 years now [10, 11]. The two basic growth processes correspond to the capture of grain boundary vacancies by diffusion, and the dilational growth of the cavities by plastic deformation of the surrounding material. We shall briefly describe various growth laws corresponding to different extremes of conditions, and then discuss how they may be combined together.

We describe cavity growth using a grain boundary areal damage fraction f [11]. This is defined as

$$f = \frac{a^2}{r_s^2} \tag{1}$$

where a is the radius of a cavity on the grain boundary, and r_s is half the average cavity spacing. It is assumed that the cavities have circular projections

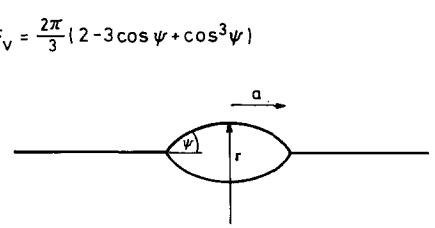

Fig. 2. Illustrating the lenticular geometry of many observed grain boundary cavities.

onto the grain boundary, and are distributed uniformly. The earliest growth law to be considered [12] involved grain boundary vacancy diffusion. The growth law is [13]

$$\dot{f} = \frac{2\pi^{3/2}\delta_b D_b \Omega C_{BN}^{3/2}(\sigma - 2\gamma/r + p)}{kTf^{1/2}\left[\ln\frac{1}{f} - \frac{1}{2}(1-f)(3-f)\right]}\left[\frac{\sin^3\psi}{F_v}\frac{4\pi}{3}\right] \quad (2)$$

where ψ is the cavity apex half angle, r is the radius of curvature of the cavity surface and $F_v r^3$ defines the cavity volume (see Fig. 2). D_b is the vacancy self diffusion coefficient in the grain boundary of width δ_b, Ω is the atomic volume, C_{BN} the cavity density on the boundary, σ the (long distance) applied tensile stress normal to the boundary, γ the surface tension and p the cavity internal gas pressure. A creep strain rate associated with this form of cavity growth is given by

$$\dot{\epsilon} = \frac{2f^{1/2}}{d(\pi C_{BN})^{1/2}}\dot{f} \quad (3)$$

where d is the grain diameter. The extension of the specimen is due solely to the opening up of the grain boundary cavities and the ductility is consequently low. No thermal creep strain need take place for this growth mechanism to operate.

Secondly, we consider cavity growth by creep deformation of the surrounding material. A number if growth laws have been suggested: the one we shall use is [11]

$$\dot{f} = 0.6\left(\frac{1}{(1-f)^m} - (1-f)\right)\dot{\epsilon}_t\left[\frac{\sin^3\psi}{F_v}\frac{4\pi}{3}\right] \quad (4)$$

where $\dot{\epsilon}_t$ is the thermal creep rate, with stress exponent m, which is usually in the range 3–5. The associated strain rate is

$$\dot{\epsilon} = \left(1 + \frac{1.2f^{1/2}}{d(\pi C_{BN})^{1/2}}\left(\frac{1}{(1-f)^m} - 1\right)\left[\frac{\sin^3\psi}{F_v}\frac{4\pi}{3}\right]\right)\dot{\epsilon}_t \quad (5)$$

which is dominated by the thermal creep rate unless f approaches unity. Failure dominated by this mechanism of cavity growth is therefore rather ductile, in contrast to the grain boundary diffusion mechanism.

A third cavity growth mechanism operates when the grain boundary is decorated with precipitates: vacancy source control [14]. Growth is by diffusion, but the supply of vacancies is controlled by dislocation climb in the boundary, and is hence linked to the thermal creep rate

$$\dot{f} = \frac{\pi^{3/2}\sin^3\psi C_{BN}^{1/2}\lambda\dot{\epsilon}_t}{6F_v f^{1/2}}\left[\frac{1-2\gamma/r\sigma + p/\sigma}{1-f}\right]^m, \quad (6)$$

and there is an associated strain given approximately by

$$\dot{\epsilon} = \dot{\epsilon}_t + \frac{2}{d}\left(\frac{f}{\pi C_{BN}}\right)^{1/2}\dot{f}. \quad (7)$$

There are further mechanisms of cavity growth in the literature, but these three seem to be sufficient for cladding materials. An approximate description of the interaction between several mechanisms has been suggested by Beeré [10], combining rates based on whether they are independent ("parallel" processes) or competing ("series"). Given the uncertainties in the individual mechanisms it is probably an adequate approximation. Fortunately, for the alloys of interest as cladding materials, it is the vacancy source control mechanism, equation (6), which controls growth in most circumstances. The time-to-fracture for creep-tested irradiated steel has been modelled with some success according to this mechanism [15] assuming a fixed number of growing cavities, and a simplified "growth impedance" network provides a good description of the failure of cladding in Fuel Cladding Transient Tests (FCTT) [16]. The overall growth rate is given by

$$\dot{f} = \dot{f}_{PG} + \frac{\dot{f}_{SC}\dot{f}_{GB}}{\dot{f}_{SC} + \dot{f}_{GB}} \quad (8)$$

where $\dot{f}_{PG}$, $\dot{f}_{SC}$ and $\dot{f}_{GB}$ are given by equations (4), (6) and (2) respectively. For simplicity, we ignore the effects of surface curvature (γ/r term) and the internal gas pressure p.

In addition, the nucleation of new cavities may be an important mechanism for damage growth [17]. The damage evolution equation would be

$$\dot{f} = \pi a^2 \dot{C}_{BN} = f\frac{\dot{C}_{BN}}{C_{BN}}. \quad (9)$$

The areal damage contribution from a freshly nucleated cavity is very small though, and this contribution to $\dot{f}$ would only be important if there were an intense burst of nucleation. Nevertheless, the evolution of the cavity density C_{BN} is important because the vacancy source control and grain boundary diffusion mechanisms both depend on this quantity. The evolution takes place either through fresh nucleation, or through the coalescence of growing cavities. If nucleation occurs with rate $\dot{C}_{BN}^{NUC}$ then the two processes give [18]

$$\dot{C}_{BN} = \dot{C}_{BN}^{NUC} - 2C_{BN}\dot{f}. \quad (10)$$

We now consider the process of cavity nucleation.

3. GRAIN BOUNDARY CAVITY NUCLEATION

Cavities usually form on the grain boundary by a vacancy condensation mechanism. Sufficient vacancies must combine by thermal fluctuation to

overcome a Gibbs free energy activation barrier consisting of surface and volume terms [19]

$$\Delta G = (3r^2\gamma - r^3\sigma)F_v. \quad (11)$$

For realistic values of surface energies and stresses, the activation energy

$$\Delta G_c = 4\gamma^3 F_v/\sigma^2 \quad (12)$$

is unattainable at reasonable temperatures unless F_v is very small or σ very large [19]. The same conclusions hold for cavities nucleated on precipitate surfaces. The implication is that nucleation occurs only when the stress is concentrated, for example by grain boundary sliding or at geometrical defects. Quite sophisticated models and calculations have been presented attempting to couple the nucleation process to a stress pulse [20–22]. The predictive value of such models is limited, however, by a lack of knowledge of the frequency and magnitude of sliding events, and a simpler model will be discussed shortly. First, though, let us see how gas in the cavity can assist nucleation. This will be useful in the next section where the effect of helium is considered. With a constant gas pressure p inside the cavity the barrier becomes

$$\Delta G = [3r^2\gamma - r^3(\sigma + p)]F_v. \quad (13)$$

One approach [23] is to assume p is kept constant as the cavity size fluctuates. The new barrier height is given by equation (12) with σ replaced by $(\sigma + p)$. An alternative is to fix n, the number of gas atoms in the cavity. Assuming ideal gas properties, ΔG becomes

$$\Delta G = (3r^2\gamma - r^3\sigma)F_v - 3nkT\ln(r/r_0) \quad (14)$$

where r_0 is a constant. The gas stabilises small cavities which would otherwise be unstable. The stable radius is given by $r = 2\gamma/p$, in the absence of an external stress. Non-ideal gas properties [24] are ignored here.

A simple model of cavity nucleation can be constructed based on the experimental observation that the nucleation rate is linearly proportional to the thermal creep rate [25]

$$\dot{C}_{BN}^{NUC} = K\dot{\epsilon}_t \quad (15)$$

where K is a constant. With cavity growth controlled by the source control of vacancies mechanism, we have, (ignoring the $(1-f)^{-m}$ factor which is relatively unimportant for most of the lifetime)

$$\dot{f} = \frac{AC_{BN}^{1/2}\dot{\epsilon}_t}{f^{1/2}} \quad (16)$$

where $A = \pi^{3/2}\sin^3\psi\lambda/(6F_v)$. Using $C_{BN} = K\epsilon_t t$, i.e. neglecting coalescence in equation (10), we obtain an approximate result for the failure strain in a constant creep rate test

$$\epsilon_f = \dot{\epsilon}t_R = \frac{f_f\left(1 + \frac{2A}{d\pi^{1/2}}\right)}{A^{2/3}K^{1/3}} \quad (17)$$

where t_R is the rupture time and f_f the failure damage fraction. A failure strain independent of stress and temperature is in agreement with the Monkman–Grant law [26]. This would also have been obtained had C_{BN} been a constant during the test. However, continuous nucleation produces a failure strain which depends on the basic parameters of both the growth mechanism (A) and the nucleation process (K). K has been estimated for various materials in Ref. [25]. The data shown in Fig. 3 follow a $\epsilon_f \propto K^{-1/3}$ correlation in agreement with equation (17).

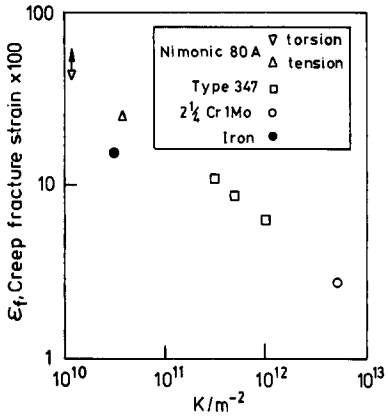

Fig. 3. Compilation of data from Dyson, showing cavity nucleation rate per unit strain against failure strain.

Samples of unirradiated 20% cw AISI 316 stainless steel generally have creep rupture strains of about 2–5%, depending on cast, and this allows K to be estimated to be about $2 \times 10^{13}\,m^{-2}$ for this material. The growth parameter A can then be estimated from equation (17). This involves the cavity apex semi-angle ψ which is commonly observed to be about 15° [27]. Using this value, we can obtain reasonable failure strains for this steel using a dislocation climb distance, λ, equal to $3\,\mu m$. Unfortunately, experimental scatter makes the fitting procedure difficult. Indeed this underlines the need to use simple models with as few parameters as possible in describing failure. For particular casts more careful assignment of values to ψ, λ and K should be made.

The above model described the nucleation of grain boundary damage in the form of both cavities and cracks. It has been recognised that the two nucleation processes should be treated similarly [28]. Nucleation is concentrated in zones where grain boundary sliding is greatest, such as boundaries parallel to the direction of applied stress, and triple-point junctions. Those cavities on the boundaries parallel to the stress axis will not grow very quickly, however, since a stress component normal to the boundary is needed. Therefore, in the absence of precipitates, deformation-driven nucleation produces cavities growing largely around triple points. Their growth and coalescence produces wedge-like cracks. In a high temperature material subject to creep, this mechanism for the formation of wedge cracks would seem to be more suitable than the Stroh condition derived for a brittle

substance [29]. Where grain boundaries contain precipitates, however, there are further potential nucleation sites for cavities. These would be more uniformly distributed, though those that grow appreciably will be located on boundaries perpendicular to the applied stress. Hence a cavity mode of damage develops. We shall consider the subsequent growth of crack and cavity damage using the same rate expressions though specific crack growth models have been formulated [30, 31]. To a geometrical constant, damage evolution by the main mechanism, vacancy source control, is the same in each mode [32].

The development so far has dealt entirely with the case of unirradiated material. However, a simple extension can be made which can begin to take into account the embrittling effect of irradiation. A link has often been drawn between this phenomenon and the formation of tiny helium-filled bubbles on the grain boundary. This gas is generated by (n, α) reactions with isotopes in the cladding, mainly ^{58}Ni and ^{10}B, [33]. Usually, these bubbles are too small to contribute to grain boundary damage, or to grow (the Hyam–Sumner instability [34]) at stresses where embrittlement is observed. We draw an important distinction, therefore, between bubbles and cavities: the latter are above a certain critical size and are able to grow. The bubbles, however, may act as nucleation sites for cavities, driven by grain boundary sliding, in a manner equivalent to the role played by precipitates. Indeed, we saw earlier that the presence of gas stabilises sub-critical cavities and reduces the nucleation barrier.

The enhancement in nucleation rate ought to depend on the bubble size and gas content, but to simplify matters we ignore this and write

$$\dot{C}_{BN}^{NUC} = K_0(c_p + C_B)\dot{\epsilon}_t \tag{18}$$

where C_B is the helium bubble density on the boundary, c_p the density of other potential nucleation sites and K_0 a constant. From equations (17) and (18) we see that the reduction in creep failure strain after irradiation is given approximately by

$$\frac{\epsilon_f^{irrad}}{\epsilon_f^{fresh}} = \left(\frac{c_p}{c_p + C_b}\right)^{1/3}. \tag{19}$$

assuming C_B is a constant. In the next section we construct a model for helium bubble nucleation which will close our set of equations.

4. HELIUM BUBBLE NUCLEATION

We shall concentrate our attention upon experiments conducted under neutron irradiation conditions, as opposed to He-implantation experiments where the helium generation rates are many orders of magnitude greater than those encountered in reactor conditions (e.g. [35–38]). We consider bubble formation to be a homogeneous nucleation process characterised by a critical cluster size and an activation barrier. The following simple equations describe the evolution of c, the density of monomeric He on the boundary, and C_B, the bubble density

$$\dot{c} = J_{He} - \pi D C_B c - \pi D c c^* \tag{20}$$

$$\dot{C}_B = \pi D c c^* \tag{21}$$

where D is the He grain boundary diffusivity and c^* is the density of critical size He clusters, represented by

$$c^* = c \exp(-G_{He}/kT) \tag{22}$$

where G_{He} is the bubble nucleation activation energy. Equation (20) specifies a helium source J_{He} and sinks comprising capture by existing bubbles [39] and homogeneous nucleation [40], respectively. The latter is of negligible importance in equation (20), so we have, for steady state conditions

$$J_{He} = \pi D C_B c \tag{23}$$

$$\dot{C}_B = \frac{J_{He}^2 \exp(-G_{He}/kT)}{\pi D C_B^2} \tag{24}$$

which at constant temperature integrates to

$$C_B = \left(\frac{3J_{He}^2 t \exp(-G_{He}/kT)}{(2\alpha + 1)\pi D}\right)^{1/3} \tag{25}$$

where a time dependence $J_{He} = J_0 t^x$ has been assumed. We can test the theory now using bubble spacing measurements [41] for an austenitic steel after thermal neutron irradiation. The average bubble separation is

$$2r_s = \frac{2}{(\pi C_B)^{1/2}} = 2\left(\frac{(2\alpha + 1)D}{3\pi^2 J_{He}^2 t \exp(-G_{He}/kT)}\right)^{1/6} \propto J_{He}^{-1/3}. \tag{26}$$

Under thermal neutron irradiation, J_{He} is proportional to f_B, the initial ^{10}B content of the steel [33], so we plot the ratios of cavity spacings against f_B in Figure 4. The data support the $J_{He}^{-1/3}$ dependence of equation (26), rather than the $J_{He}^{-1/4}$ prediction of Ref. [42].

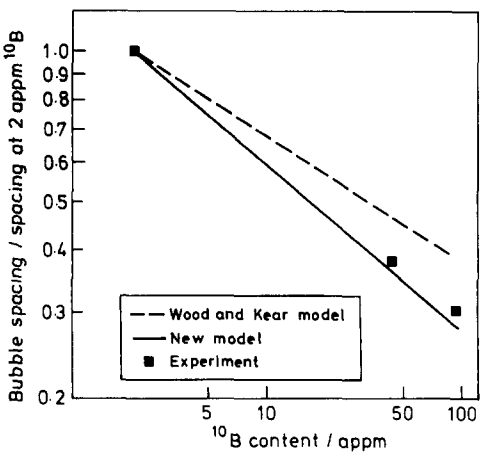

Fig. 4. Dependence of helium bubble spacing on ^{10}B content of irradiated austenitic steels.

To proceed further we assume that in-pile creep rupture lifetimes at low stresses are dominated by the time required for bubbles to grow to the Hyam–Sumner bubble instability, also known as spontaneous cavity nucleation from bubbles [43], or gas-driven rupture [44]. This idea has been developed previously [44] in order to account for the difference in behaviour between equivalent creep rupture tests in and out of pile. The instability requires sufficient gas in each bubble to eliminate the activation barrier ΔG_c. From equation (14) the number of He atoms per bubble, n, needs to reach a critical value

$$n^* = \frac{32F_{vB}\gamma^3}{27kT\sigma^2} = \frac{Q}{\sigma^2} \tag{27}$$

using ideal gas properties. F_{vB} is the bubble volume factor, analogous to F_v. The time to rupture t_R can then be found from

$$n^* = \int_0^{t_R} J_{He}\,dt/C_B = \left(\frac{(2\alpha+1)\pi DJ_0}{3\exp(-G_{He}/kT)}\right)^{1/3} \times \frac{t_R^{(\alpha+2)/3}}{\alpha+1} = \frac{Q}{\sigma^2}. \tag{28}$$

Hence

$$t_R = [(\alpha+1)Q]^{3/(2+\alpha)} \frac{1}{\sigma^{6/(2+\alpha)}} \times \left(\frac{3\exp(-G_{He}/kT)}{(2\alpha+1)\pi DJ_0}\right)^{1/(2+\alpha)}. \tag{29}$$

The gas flux to the grain boundary may be modelled assuming an idealised spherical grain with uniform internal He generation

$$J_{He} = \frac{4}{\pi^{1/2}}\frac{P}{\Omega}(D_g t)^{1/2} = J_0 t^{1/2}. \tag{30}$$

With $\alpha = 1/2$ equation (29) gives $t_R \propto \sigma^{-2.4}$. Experimentally [45], in-pile rupture times are characterised by a stress exponent of -2.5, in agreement with this model. Equation (30) is the solution, for constant P, of the equation

$$\frac{\partial c_g}{\partial t} - \frac{1}{R^2}\frac{\partial}{\partial R}\left(D_g R^2 \frac{\partial c_g}{\partial R}\right) = \frac{P}{\Omega} \tag{31}$$

where c_g is the intragranular He concentration and R is radial distance in the grain. The boundary condition used is $c_g(R = d/2) = 0$ where d is the grain diameter. Ω is the atomic volume, P the He generation rate in atoms/atom/s and D_g is the matrix helium diffusivity. This latter quantity has been measured experimentally

$$D_g \approx \begin{cases} 6.3\times10^{-7}\exp(-9391/T). & T \geqslant 750°C\ [46] \\ 0.9\times10^{-4}\exp(-33620/T), & T \leqslant 750°C\ [47]. \end{cases} \tag{32}$$

Experimentally, the activation temperature for in-pile rupture times of several cladding materials is about 33040K [45, 48]. Using equation (29) with $\alpha = 1/2$ and D_g for $T \leqslant 750°C$ we can deduce that

$$D \propto \exp(-65855/T)\exp(-G_{He}/kT) \tag{33}$$

and substituting into equation (25) we find that the bubble density C_B has a temperature dependence proportional to $\exp(10783/T)$. Measurements of C_B [35] indeed show a low sensitivity to temperature. The high activation temperature in equation (33) deserves some comment. The migration mechanism may be controlled by He trapping at strong-binding sites on the grain boundary. The grain boundary diffusivity has not been measured for He in steels, however, so we cannot test this prediction. We assume that equation (33) holds for all temperatures.

Our model now produces the correct temperature and stress dependence of the in-pile rupture times

$$t_R = t_0\sigma^{-2.4}\exp(33043/T). \tag{34}$$

The constant t_0 is found by fitting equation (25) to bubble density data for 2 ppm ^{10}B steel irradiated at 650°C [41]. The observed bubble spacing of 0.53 μm is obtained with

$$D = 7.175\times10^{23}D_g\exp(-32232/T) \times \exp(-G_{He}/kT) \tag{35}$$

so using $\gamma = 2J\ m^{-2}$. $P = 3\times10^{-13}\,s^{-1}$, $\Omega = 8\times10^{-30}\,m^3$, $T = 650°C$ in equation (29) we get $t_0 = 1.75\times10^{11}F_{vB}^{6/5}$: Equation (25) then gives, for $\sigma = 100$ MPa and $T = 650°C$, a rupture time $t_R = 1.083\times10^4 F_{vB}^{6/5}$ h. The experimental rupture time for an austenitic steel under these conditions is 5.5×10^3 h [45], so we conclude that $F_{vB} = 0.57$ and $\psi_B = 47°$, which is an acceptable bubble apex half angle, and $t_0 = 8.9\times10^{10}$s. Now we have

$$C_B = 1.44\times10^{-8}(Pt/\Omega)^{2/3}\exp(10783/T) = 3.6\times10^7\exp(10783/T)H^{2/3}\,m^{-2} \tag{36}$$

where $H = Pt$ is the total fractional helium implantation in appm.

The fractional grain boundary area occupied by the bubbles is given by $f = \pi r^2 C_B \sin^2\psi_B$. Assuming the bubbles are in equilibrium we have

$$\frac{2\gamma}{r} = \frac{nkT}{F_{vB}r^3} \tag{37}$$

where, again, ideal gas properties are assumed. Hence

$$f = \frac{\pi kT\sin^2\psi_B}{2F_{vB}\gamma}nC_B = \frac{\pi kT\sin^2\psi_B}{2F_{vB}\gamma}\int J_{He}\,dt \tag{38}$$

$$f \approx 1.81\times10^{-2}T\exp(-16812/T)(H/appm)t^{1/2}. \tag{39}$$

At 650°C, and with 13 appm of generated He after 1 year in a fast reactor, this gives $f \approx 0.016$. This would be a starting condition for the growth law

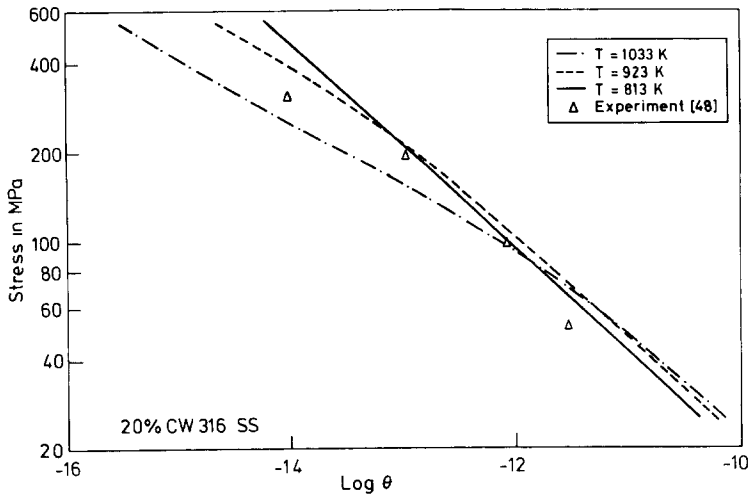

Fig. 5. Unirradiated creep rupture times: Dorn parameter against stress.

equation (8), assuming the stress became high enough to destabilise the whole of the population of bubbles. The projected bubble radius in the grain boundary is

$$a = 1.27 \times 10^{-5}\, T^{1/2} \times \exp(-13798/T)(\mathrm{H/appm})^{1/6}\, t^{1/4}\,\mathrm{m} \quad (40)$$

which is about 14 nm for the example given. The evolving Hyam–Sumner stress σ_c above which bubbles become unstable can then be written [42]

$$\sigma_c = \frac{4\gamma \sin \psi_B}{3\sqrt{3}a}. \quad (41)$$

5. CALCULATIONS OF RUPTURE TIMES

We now have all the equations describing intergranular rupture: cavity nucleation [equation (18)], growth [equation (8)] and coalescence [equation (10)] and bubble nucleation [equations (20, 21, 31)]. In addition spontaneous cavity nucleation from bubbles is modelled by monitoring the gas content of each bubble. There remain the initial conditions, which fortunately turn out not to be important. We use an initial damage fraction of 10^{-5} and an initial cavity density of $5 \times 10^9\ \mathrm{m}^{-2}$. Comparison with experiment is then possible by specifying the creep rate $\dot{\epsilon}_t$ and the He generation rate P. The fully time-dependent theory covers three classes of creep rupture experiments: unirradiated, in-pile and post-irradiation creep tests.

We are primarily interested in 20% cw AISI 316 steel, for which we use a creep rate for $T > 600°C$ given in s^{-1} by

$$\dot{\epsilon}_t = 3.3 \times 10^5 (1 + 6.2 \times 10^{-5}\, t^{0.75}) \times \exp(-54241/T)(\sigma/\mathrm{MPa})^5. \quad (42)$$

The time-dependent acceleration term represents the slow recrystallisation of the cold worked material at high temperature [48]. The following comparisons with experiment all refer to this material. Using parameters defined earlier we can calculate a time-to-rupture, which occurs when the damage exceeds a failure fraction f_f. The damage rate accelerates when f becomes large, so the results are not too sensitive to this threshold: we use $f_f = 0.6$. Calculated unirradiated times-to-rupture at various temperatures and stresses are given in Fig. 5 in the form of the Dorn parameter defined by $\theta = t_R \exp(-Q_R/T)$ with $Q_R = 33{,}043\mathrm{K}$. Experimental data from Ref. [49] lie on a single line with this value of Q_R, the trend of which is shown. The calculations show a temperature dependence in agreement with the data which can be demonstrated analytically. With suitable approximations it can be shown that, for low stress tests

$$t_R \propto \sigma^{-20/7} \exp[4Q_c/(7T)] \quad (43)$$

where Q_c is the creep activation temperature in equation (42). This gives a Q_R of 30,995K which is close to the experimental value. For higher stresses, we have $t_R \propto \sigma^{-5} \exp(Q_c/T)$. This behaviour would apply for all stresses if the creep rate $\dot{\epsilon}_t$ were given by the more standard time-independent form.

We next simulate in-pile creep tests. We again use a He generation rate of 13 appm/year. The calculated times-to-rupture are given in Fig. 6, this time in terms of a Larson–Miller parameter, defined as [50]

$$\mathrm{LMP} = T(13.5 + \log_{10} t_R) \quad (44)$$

where t_R is in hours. Unirradiated and in-pile rupture results are given in Fig. 6 to illustrate the reduced lifetime (and ductility) of the material tested in-reactor. Fits to the parameters c_p and K_0: of $2 \times 10^{11}\ \mathrm{m}^{-2}$ and 100 were used, respectively. At low stresses, the failure times are dominated by the time to nucleate cavities from He bubbles, and so they follow a $\sigma^{-2.4}$ dependence.

The third class of test involves irradiation followed by an out-of-pile creep test outside the reactor, Figure 7 shows the trend of times-to-rupture compared with experimental data [51]. Also shown are the

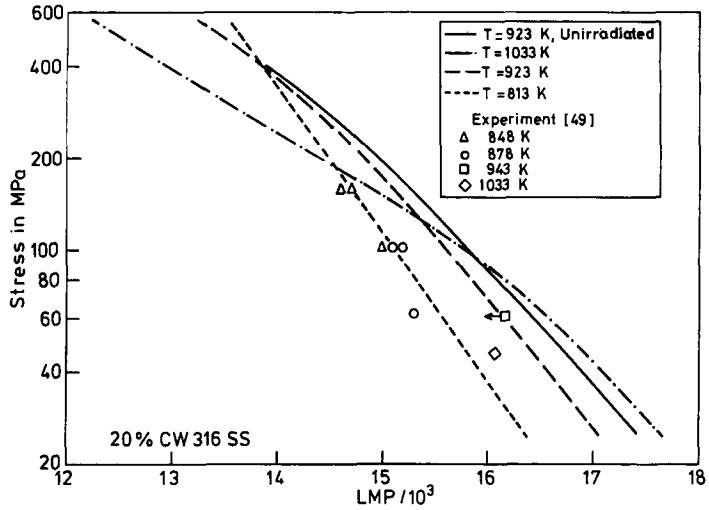

Fig. 6. In-pile and unirradiated creep rupture times: Larson–Miller parameter against stress.

unirradiated rupture times; calculated and experimental. The irradiated materials were injected with He at 650°C and 13 appm/year for periods of about six months and one year. The embrittlement of the material is more extreme at stresses higher than about 80 MPa, which is the calculated value of the Hyam–Sumner stress after such an irradiation. The data shown illustrate cast-to-cast variability.

Finally, we examine Fuel Cladding Transient tests (FCTT). Here, the stress is kept constant but the temperature is ramped to cause fracture at a failure temperature. Some comparisons between calculations and experiments [52] are given in Fig. 8, showing good agreement.

6. CONCLUSIONS

Reactor pin cladding failure experiments have generally been interpreted using empirical rules. This work has sought to strengthen our understanding of fracture process by developing theories of the underlying physics. This has involved the formulation of simple equations which provide analytical expressions for failure characteristics, and which can be solved numerically for varying conditions, an aspect which has been missing in the past [53, 54].

The failure mechanism we have considered here is the intergranular mechanical rupture mode. The transgranular mode has been developed in parallel and is described elsewhere [9]. Both models are included in a computer program CITRUS (Cladding Intergranular and Transgranular RUpture Subroutine) which has been included in the TRAFIC and TRANSURANUS fuel pin behaviour codes. The complexity of the fracture process has required an appeal to experiment to fix parameters. The observed unirradiated failure strains fix the nucleation rate parameters and the dislocation climb distance. Experimental helium bubble densities and low stress in-pile rupture times fix the form of the grain boundary

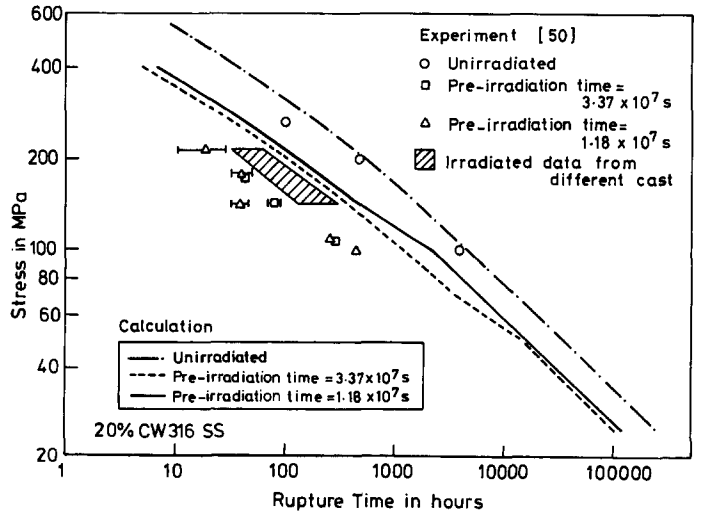

Fig. 7. Post irradiation creep rupture times.

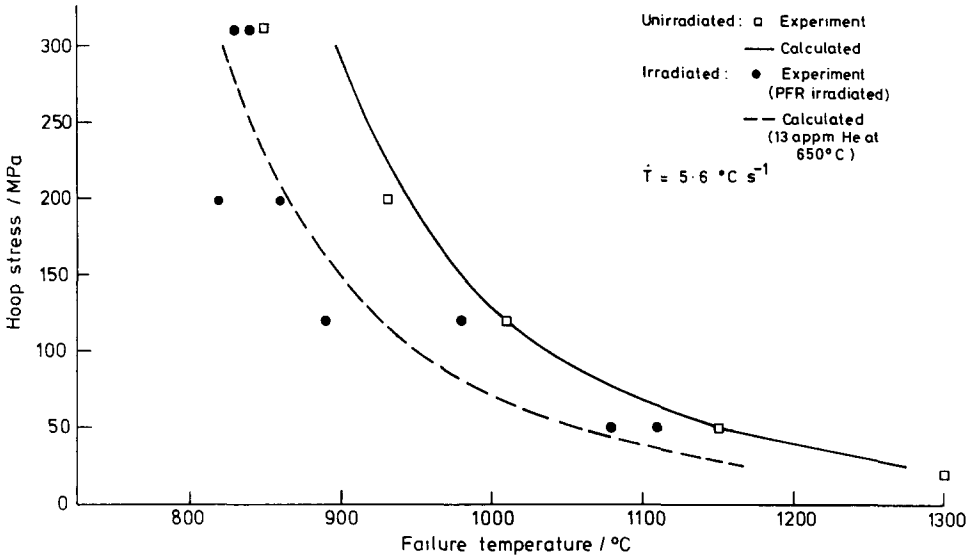

Fig. 8. Failure temperatures against initial stress in FCTT tests.

helium diffusivity. Finally, the initial density of potential cavity nucleation sites C_p is set by considering the ductility loss due to irradiation. The unknown parameters are therefore chosen using quite different sets of experimental data, and the models can then be tested against a large body of experiments: creep rupture tests on unirradiated and irradiated material, both inside and outside a reactor, as well as FCTT tests.

We have modelled in detail the nucleation of helium bubbles on grain boundaries. This gives rise to the phenomenon of helium embrittlement, which, in our model, is due to the enhancement of the nucleation rate of grain boundary cavities. It is important to distinguish bubbles, which is terms of grain boundary damage are essentially benign, from cavities, which have overcome an energy barrier and are free to grow by vacancy absorption. The bubble nucleation problem is modelled by a homogeneous nucleation theory involving the diffusion of helium into the grain boundaries to nucleate bubbles or to be absorbed by existing bubbles. The model takes bubble nucleation to be a continuous process throughout irradiation. Similarly, cavity nucleation is continuous, and is proportional to the creep rate. No attempt is made to model the underlying vacancy condensation in cavity nucleation, in a manner similar to the homogeneous nucleation model applied to bubble formation, since the phenomenon is much more stress-dependent, and controlled by ill-defined sliding occurring on the grain boundary. The bubble nucleation problem would seem to be helium supply controlled. However, one mechanism for cavity nucleation is modelled microscopically: spontaneous nucleation from bubbles when the Hyam–Sumner stress is exceeded. Once nucleated, either at an intrinsic potential nucleation site, such as a triple point or precipitate, or at a bubble, a cavity grows and damages the load-bearing strength of the boundary. Fracture occurs at a critical fractional areal damage.

The theories of nucleation and growth take into account the phenomenology of intergranular fracture and account for a number of experimental trends. Amongst these are the ^{10}B dependence of bubble densities in irradiated steels, the formation of wedge cracks at triple points and cavities on boundaries perpendicular to the stress, and the stress dependence of in-pile rupture times. We also gain insight into the Dorn and Larson-Miller parameter life fraction approaches.

The enhancement of the cavity nucleation rate due to the presence of helium bubbles is the most novel aspect of this work. It is based on a simplified picture: that the nucleation is proportional to the number of potential cavity sites available, for a given increment of grain boundary deformation, and that a helium bubble is such a site, independent of its size. This latter point is a gross simplification: small bubbles are less effective than larger ones, but the formulation has an appealing simplicity and allows some analytical results to be derived. Moreover, the data are not inconsistent with the approximation.

Acknowledgements—This work was supported in part by the Commission of the European Communities, Joint Research Centre, Ispra Establishment, and in part by the Underlying Research Programme of AEA Technology. The author thanks Dr J. R. Matthews for useful discussions.

REFERENCES

1. D. R. Harries. Harwell Rep. AERE-R9179.
2. J. R. Matthews, R. F. Cameron, P. E. Coleman and R. Thetford, *BNES Conf. On Fast Reactor Safety*, Guernsey, U.K.(1986).
3. K. Lassmann and H. Blank, *Nucl. Engng Design* **106**, 291 (1988).

4. G. Van Goethem, A. Clusaz, J. Devos, H. Nguyen, J. Reyner, A. Sola and H. U. Wider, *BNES Conf. on Fast Reactor Safety*, Guernsey, U.K. (1986).
5. T. Preusser, Tech. Univ. Darmstadt Rep. rtda-98-93 (1983).
6. T. Preusser and H.-P. Schiffer, *8th Int. Conf. on Structural Mechanics in Reactor Technology*, Brussels, August, paper C2/8 (1985).
7. J. R. Matthews and T. Preusser, *Nucl. Engng Design* **101,** 281 (1987).
8. I. J. Ford and J. R. Matthews, *Proc. 19th Canadian Fracture Conf., Ottawa* (edited by A. S. Krausz, J. I., Dickson, J-P. A. Immarigeon and W. Wallace), Kluwer Academic (1989).
9. I. J. Ford, *J. nucl. Mater.* **182,** 52 (1991).
10. W. Beeré, in *Cavities and Cracks in Creep and Fatigue* (edited by J. H. Gittus). Appl. Sci. London (1982).
11. A. C. F. Cocks and M. F. Ashby, *Progr. Mater. Sci.* **27,** 189 (1982).
12. D. Hull and D. E. Rimmer, *Phil. Mag.* **4,** 673 (1959).
13. M. V. Speight and W. Beeré, *Metal Sci.* **9,** 190 (1975).
14. W. Beeré, *J. Mater Sci.* **15,** 657 (1980).
15. K. L. Kear and M. H. Wood, Harwell Rep. AERE-R10907 (1983).
16. N. S. Cannon, C. W. Hunter, K. L. Kear and M. H. Wood, *J. nucl. Mater.* **139,** 60 (1986).
17. G. W. Greenwood, *Phil. Mag.* **19,** 423 (1969); D. A. Woodford, *Metal Sci.* **3,** 349 (1969).
18. D. S. Wilkinson, *Acta metall.* **35,** 1251, 2791 (1987).
19. R. Raj and M. F. Ashby, *Acta metall.* **23,** 653 (1975).
20. J. N. Al-Hajji, Ph. D. thesis, UCLA-ENG-8533 (1985).
21. J. S. Wang, J. J. Stephens and W. D. Nix, *Acta metall* **33,** 1009 (1985).
22. M. H. Yoo and H. Trinkaus, *Metall. Trans.* **14A,** 547 (1983).
23. H. Trinkaus and H. Ullmaier, *Phil. Mag.* **A39,** 563 (1979).
24. R. L. Mills, D. H. Leibenberg and J. C. Bronson, *Phys. Rev.* **B21,** 5137 (1980).
25. B. F. Dyson, *Scripta metall.* **17,** 31 (1983).
26. F. C. Monkman and N. J. Grant, Proc. ASTM56, p. 593 (1956).
27. P. J. Clemm and J. C. Fisher, *Acta metall.* **3,** 70 (1955).
28. R. D. Nicholson and C. L. Formby, *Int. J. Fract.* **11,** 595 (1975).
29. A. N. Stroh, *Proc. R. Soc.* **223A,** 404 (1954); *Adv. Phys.* **6,** 418 (1957).
30. W. D. Nix, D. K. Matlock and R. J. Dimelfi, *Acta metall.* **25,** 495 (1977).
31. D. S. Wilkinson and V. Vitek, *Acta metall.* **30,** 1723 (1982).
32. W. Beeré and M. V. Speight, *Metal Sci.* **12,** 593 (1978).
33. I. R. Birss, *J. nucl. Mater.* **34,** 241 (1970).
34. E. D. Hyam and G. Sumner, Radiation Damage in Solids 1, IAEA, Vienna, p. 233 (1962).
35. P. L. Lane and P. J. Goodhew, *Phil. Mag.* **A48,** 965 (1983).
36. H. Schroeder, P. Batfalsky, *J. nucl. Mater.* **117,** 287 (1983); P. Batfalsky and H. Schroeder, *J. nucl. Mater.* **122 & 123,** 1475 (1984).
37. H. Ullmaier, *Radiat. Eff.* **101,** 147 (1986).
38. C. Brown, R. M. Sharpe, E. J. Fulton and C. Cawthorne, *BNES Conf. on Dimensional Stability and Mechanical Behaviour of Irradiated Metals and Alloys.* Brighton, Vol. 1, p. 63 (1983).
39. M. H. Wood, Harwell Rep. TP988 (1983).
40. R. Becker and W. Döring, *Ann. Physik* **21,** 719 (1935).
41. D. R. Harries, A. C. Roberts, G. T. Rogers, J. D. H. Hughes and M. A. P. Dewey, *Radiation Damage in Reactor Materials*, IAEA-SM-120/G-5, Vienna, Vol., 2, p. 357 (1969).
42. M. H. Wood and K. L. Kear, *J. nucl. Mater.* **118,** 320 (1983).
43. K. C. Russell, *Acta metall.* **26,** 1615 (1978); C. A. Parker and K. C. Russell, in *Effects of radiation on Materials: Eleventh Conf.* (1982) (edited by H. R. Brager and J. S. Perrin), ASTM STP 782, p. 1042.
44. R. Bullough, D. R. Harries and M. R. Haynes, *J. nucl. Mater.* **88,** 312 (1980).
45. C. Wassilew, W. Schneider and K. Ehrlich, *Radiat. Eff.* **101,** 201 (1986).
46. V. Philipps, K. Sonnenburg and J. M. Williams, *J. nucl. Mater.* **107,** 271 (1982).
47. M. B. Lewis and K. Farrell, *Nucl. Inst. Meth. Phys. Res.* **B16,** 163 (1986).
48. J. Standring, A. M. Wilson and M. C. Clayden, *BNES Conf. on Dimensional Stability and Mechanical Behaviour of Irradiated Metals and Alloys*, Brighton (1983).
49. A. J. Lovell, B. A. Chin and E. R. Gilbert, *J. Mater. Sci.* **16,** 870 (1981).
50. R. J. Pugh and M. L. Hamilton, in *Influence of Radiation on Material Properties: 13th Int. Symp.*, Part II (edited by F. A. Garner, C. H. Henager Jr and N. Igata), ASTM STP 956, p. 22. Philadelphia, Pa (1987).
51. R. L. Fish, *Nucl. Technol.* **35,** 9 (1977).
52. C. W. Hunter, R. L. Fish and J. J. Holmes, *Nucl. Technol.* **27,** 376 (1975).
53. H. Trinkaus, *J. nucl. Mater.* **118,** 39 (1983).
54. H. Trinkaus, *J. nucl. Mater.* **133 & 134,** 105 (1985).

APPENDIX

Nomenclature

a = cavity radius projected onto boundary
c = grain boundary helium density
c^* = grain boundary critical helium cluster density
c_g = intragranular helium density
c_p = grain boundary precipitate density
C_B = grain boundary bubble density
C_{BN} = grain boundary cavity density
d = grain diameter
D = grain boundary helium diffusivity
D_b = grain boundary vacancy self diffusion coefficient
D_g = intragranular helium diffusivity
f = grain boundary areal damage fraction
f_B = fractional ^{10}B content
F_v = cavity volume factor
F_{VB} = bubble volume factor
G_{HE} = activation energy for bubble formation
H = total generated helium
J_{HE} = helium flux to grain boundary
k = Boltzmann's constant
K = cavity nucleation rate per unit creep rate
LMP = Larson–Miller parameter
m = stress exponent in creep rate
n = number of helium atoms per bubble
n^* = critical n for Hyam–Sumner instability
p = gas pressure in bubble-cavity
P = helium generation rate
r = radius of curvature of bubble-cavity surface
r_s = bubble/cavity separation on grain boundary
R = radial coordinate in grain
t_R = time to rupture
T = temperature
α = time exponent in J_{He}
γ = surface tension
δ_b = thickness of grain boundary
$\dot{\epsilon}_t$ = thermal creep rate
$\dot{\epsilon}$ = strain rate
ϵ_f = failure strain (ductility)
λ = dislocation climb distance
ψ = cavity apex half-angle
ψ_B = bubble apex half-angle
σ = stress
θ = Dorn parameter
Ω = lattice atomic volume